HHS Public Access

Author manuscript

Magn Reson Med. Author manuscript; available in PMC 2018 November 01.

Published in final edited form as:

Magn Reson Med. 2017 November ; 78(5): 1900–1910. doi:10.1002/mrm.26585.

Positive Contrast from Cells Labeled with Iron Oxide Nanoparticles. Quantitation of Imaging Data

Sergey Magnitsky[1], **Jinjin Zhang**[2], **Djaudat Idiyatullin**[2], **Geetha Mohan**[3], **Michael Garwood**[2], **Nancy E. Lane**[3], and **Sharmila Majumdar**[1]

[1]Musculoskeletal Quantitative Imaging Research, Department of Radiology and Biomedical Imaging, University of California, San Francisco, USA

[2]Center for Magnetic Resonance Research and Department of Radiology, University of Minnesota, Minneapolis, MN, USA

[3]Center for Musculoskeletal Health, University of California at Davis School of Medicine, Sacramento, CA 95817, USA

Abstract

Purpose—Conventional T2-weighted MRI produces a hypointense signal from iron-labeled cells, which renders quantification unfeasible. We tested SWIFT MRI pulse sequence to generate a quantifiable hyperintense signal from iron-labeled cells.

Methods—Mesenchymal stem cells (MSCs) were labeled with different concentrations of iron oxide particles and examined for cell viability, proliferation, and differentiation. The SWIFT sequence was optimized to detect and quantify the amount of iron in the muscle tissue after injection of iron oxide solution and iron-labeled MSCs.

Results—The incubation of MSCs with iron oxide and low concentration of poly-L-lysine mixture resulted in an internalization of up to 22 pg of iron per cell with no adverse effect on MSCs. Phantom experiments showed a dependence of SWIFT signal intensity on the excitation flip angle. The hyperintense signal from iron-labeled cells or solutions was detected and an amount of the iron oxide in the tissue was quantified with variable flip angle method.

Conclusions—The SWIFT sequence can produce a quantifiable hyperintense MRI signal from iron-labeled cells. The graft of 18×10^6 cells was detectable for 19 days after injection and amount of iron was quantifiable. The proposed protocol simplifies the detection and provides a means to quantify cell numbers.

Keywords

iron oxide; SWIFT; cell tracking; positive contrast; hypointense signal intensity

The correspondence should be directed to: Sergey Magnitsky PhD, Dept. Radiology, UCSF, 185 Berry St., Suite 350, San Francisco, CA, 94107, Phone: (415)-514-8233, sergey.magnitsky@ucsf.edu.

Introduction

The ability of mesenchymal stem cells (MSCs) to differentiate into osteoblasts (bone cells), chondrocytes (cartilage cells), myocytes (muscle cells) and adipocytes (fat cells) makes them very attractive for the treatment of bone disorders [1]. Therapeutic effects were observed in pre-clinical studies in which MSC treatment was used for bone fractures [2], osteoarthritis [3] and osteoporosis [4]. Although the translation of MSC therapy for bone disorders into the clinic is promising [5], human studies of MSC treatment of bone diseases will require a reliable and noninvasive technique to monitor cells after transplantation.

Of the many methods used to image grafted cells, magnetic resonance imaging (MRI) has shown the most promising results [6]. Its success is due to high spatial resolution, superior soft-tissue contrast, and availability of efficient contrast agents, the most promising of which is iron oxide nanoparticles [6]. Labeling cells with these particles provides very high sensitivity and single cell detection has been reported [7]. Iron-oxide labeled cells were used in the first trial of *in vivo* detection of grafted stem cells in human [8–11]. However, the hypointense (negative) signal produced by iron-labeled cells is challenging to detect and quantify in the areas of MR images with low signal intensity, such as bone. The determination of the amount of the grafted cells in the target tissue is critically important for the prediction of therapeutic effect, and several techniques were developed to transform hypointense signal intensity from iron-labeled cells into a hyperintense signal using off-resonance RF excitation of water [12, 13], echo-shifts in k-space [14], or additional refocusing gradients [15]. These MRI techniques have potential but need further development, especially in quantification procedures.

Several methods have been developed to detect MR signals from fast relaxing spins, which can also be used to generate hyperintense signal intensity from iron-labeled cells such as Ultrashort Echo Time (UTE) [16–19], Zero Echo Time -ZTE [20–23], ZTE combined with Single Point Imaging (SPI) [24], and SWeep Imaging with Fourier Transformation (SWIFT) [25]. ZTE-based methods require very short RF pulses and often use low flip angles that result in a relatively low signal to noise ratio [26, 27]. Due to T2 decay of signal during the gradient ramp time, the UTE sequence cannot be used effectively for imaging objects with extremely short T2 (T2<200 microseconds) [28]. The SWIFT pulse sequence was introduced to image tissues with very short T2 relaxation time. This pulse sequence utilizes swept RF excitation and virtually simultaneous signal acquisition in a time-shared mode in the presence of imaging gradients. This approach allows the detection of NMR signal from spins with ultra-short T2, reduced demand on the field gradient efficiency and low peak amplitude of RF pulses. [25, 29–32]. The SWIFT method has been successfully implemented for imaging dental tissue [29, 33], lung parenchyma [34], brain calcifications [35], and mandibular invasion by carcinoma [30]. Two methods for the quantification of SWIFT NMR signals from fast relaxing spins, such as iron oxide solutions were published recently [36, 37]. One study used SWIFT to detect iron-oxide-labeled stem cells that were injected into the myocardium of rats [38].

The goals of the present study were to evaluate the feasibility of using SWIFT MRI to produce a hyperintense signal from iron-labeled MSCs *in vivo,* and to quantify the amount

of iron in the injected area. To accomplish these goals, we conducted *in vitro* experiments to identify a range of iron oxide particle concentrations that would not reduce the viability of the MSCs and would produce a sharp hyperintense MRI signal from labeled cells. After that, we acquired *in vivo* images of grafted MSCs in the muscle tissue of mice and quantified the amount of iron in the injection site over time.

Methods

Cells

Mouse Mesenchymal Stem Cells (MSCs) for this study were obtained from Dr. N. E. Lane laboratory (Center for Musculoskeletal Health, the University of California at Davis School of Medicine, Sacramento, CA, USA). Cells were maintained on uncoated T-75 plastic flasks and split at a ratio of 1:10, once a week by gentle trypsinization and 700 rpm centrifugation for 2 min. Minimum Essential Medium α (MEM α) with 10% fetal bovine serum (FBS) and 1% Antibiotic-Antimycotic (PSA) supplements were used as growth media.

Labeling of cells with iron oxide particles

Iron oxide particles that have been approved by the FDA for human use were utilized in this study (Feraheme, Amag, Waltham, MA, USA). To label MSCs, the iron oxide particles were mixed with the growth media at the following concentrations: 12, 25, 50, 100, 200, 400, 500, 800, 1000 μg/ml and added into flasks with adherent cells, incubated overnight, and washed three times with phosphate buffered saline (PBS). Labeled cells were harvested by gentle trypsinization and centrifugation and kept on ice till future experiments. To improve intracellular uptake of the iron oxide particles, Feraheme was mixed with poly-L-lysine (PLL, Sigma, St. Louis, MO, USA). We tested both low and high concentrations of the transfection agent PLL in our experiments. For the low transfection agent mixture, we added 375 ng of PLL for each 50 μg of Feraheme and stirred the mixture at room temperature for 60 min [39–41]. For the high transfection agent mixture we added 3750 ng of PLL for every 50 μg of Feraheme and stirred the mixture at room temperature for 60 min. Fe-PLL mixtures were then added to MSCs and incubated overnight. After incubation, the labeled cells were washed with PBS, harvested and kept on ice till needed. Intracellular concentrations of iron in MSCs were measured by inductively-coupled mass spectroscopy method at UC Davis chemistry core facility [42].

The viability of iron-labeled MSCs

A higher concentration of iron oxide particles has been shown to be better for detecting grafted cells with T2-weighted imaging [43]; however, an excess of the contrast agent can be toxic for the donor cells. To determine non-toxic concentrations of the iron oxide for MSCs, that are sufficient for generating a hyperintense signal, we incubated MSCs with several concentrations of Feraheme and Feraheme-PLL mixtures. We performed a colorimetric assay to measure the metabolic activity of mitochondria to determine if there was a toxic effect from the iron oxide particles. MSCs were seeded into a 96-well flat bottom plate at ~60% confluency and cultured for 3–4 hours with 100μl of growth media per well. After the cells' attachment, Feraheme or Feraheme-PLL mixtures were added with final concentrations of 12, 25, 50, 100, 200, 400, 500, 800, 1000 μg/ml of iron oxide and cells

were incubated overnight at 37 °C and 5 % of CO_2. The following day, cells were washed three times with PBS to remove free iron oxide and the cell viability assay was performed according to the manufacturer's protocol ("Cell Proliferation Reagent WST-1", Sigma-Aldrich). Briefly: 10 μl of WST-1 reagent was added per well and incubated for 4 hours at 37 °C and 5 % of CO_2. As a negative control, 3 wells with unlabeled MSCs were treated for 3 hours with 400 μM of temozolomide (TMZ, which is cytotoxic at higher concentrations). The cell proliferation reagent containing a tetrazolium salt WST-1, was used for the measurement of cell viability in cytotoxicity studies. The tetrazolium salt was cleaved to formazan by cellular enzymes and the expansion in the number of viable cells resulted in an increase in the overall activity of mitochondrial dehydrogenases in the sample. This change in enzyme activity led to an increase in the amount of formazan dye formed which directly correlated to the number of metabolically active cells in the culture. Quantification of the formazan dye produced by metabolically active cells was performed optically using an ELISA reader at 440 nm after vigorous shaking of the plate for 1 min. To determine the long-term effect of the iron oxide particles on MSCs, viability tests were also conducted at 1, 5, 10 and 21 days after iron labeling.

Differentiation of iron-labeled MSC

To measure the effect of iron oxide particles on osteoblast differentiation, MSCs were incubated overnight with 0, 50, 100, 200, 400 μg/ml Feraheme and low concentration of PLL (375 ng of PLL for each 50 μg of Feraheme). After washing with PBS, MSCs were seeded at 60% confluence in 24 well plates. Twelve hours later, regular growth media was replaced with the differentiation medium and cells were allowed to proliferate/differentiate. The differentiation media contained: α-MEM, 10%FBS, 1%PSA, 50μg/ml VitC and 10mM glycerol phosphate. The differentiation media was changed every 3 days. After 21 days of the proliferation/differentiation, Alizarin Red Staining (Alizarin Red S Staining Quantification Assay, ScienCell) was performed to detect osteoblasts in the culture as described earlier [44]. The number of MSCs that had differentiated into osteoblasts (alizarin positive) was determined optically at wavelength λ = 405 nm.

Phantom preparation

To evaluate the ability of SWIFT sequence to generate hyperintense MRI signal, a phantom with several concentrations of the iron oxide particles was prepared. The stock solution (30 mg/ml) was diluted several times with PBS to produce 0, 25, 50, 100, 200, 300, 600, 1200 and 30000 μg/ml solutions and was transferred into 200 μl mini-Eppendorf tubes. The tubes were placed into a custom made holder and positioned in the RF coil.

Cell pellet phantom preparation

To evaluate the relationship between R1-relaxivity and the iron oxide concentration inside the MSCs, phantoms with a different number of cells were prepared. 1×10^6, 2×10^6 and 3×10^6 cells were incubated with 50 μg/ml of iron oxide and 375 ng/ml of PLL overnight. The following day, the cells were trypsinized, washed with PBS three times and transferred to 200μl Eppendorf tubes. Tubes were centrifuged at 1200 rpm, the cell pellets were imaged and R1 maps were reconstructed. R1-value of the pellet with three million unlabeled cells was measured as well.

In vivo imaging of mice after injection of the iron oxide solution

All procedures were conducted in accordance with the National Institute of Health Guide for the Care and Use of Laboratory Animals and were approved by the Institutional Animal Care and Use Committee of the University of California at San Francisco. In order to demonstrate that positive contrast can be generated using the SWIFT-imaging protocol *in vivo*, 50 μl of 50 μg/ml Feraheme solution was injected with 28-gauge needle intramuscularly in the hindlimb of adult female BALB/c mice (n=3, 25–35 g). Mice were anesthetized with a mixture of 2% isoflurane and pure oxygen that was delivered to the animal with 0.6 liters per hour rate and *in vivo* imaging experiments were performed approximately one hour post-injection.

In vivo Implantation of MSCs

18×10^6 MSCs labeled with 200 μg/ml of iron oxide were re-suspended in 100 μl of PBS and injected intramuscularly in the hindlimb of adult female BALB/c mice (n=3). *In vivo* MR imaging was performed approximately one hour after injection and at 3, 10 and 19 days after injection of iron-labeled cells. The primary goal of this study was to test the capability of the SWIFT sequence to produce a quantifiable hyperintense signal from iron-labeled MSCs. We injected the large number of MSCs to minimize difficulties associated with sensitivity of the method.

MR imaging

All imaging experiments were performed with a horizontal bore 7 T magnet interfaced with Agilent console (Agilent/Varian, Santa Clara, CA). Images of the phantom were acquired with a 38 mm ID Agilent quad birdcage coil. *In vivo* imaging of mouse hindlimbs were performed with a 2 cm surface coil. Positions of the phantom or animals were determined with a gradient echo pulse sequence using the following parameters: repetition time (TR) 10 msec, echo time (TE) 4 msec, excitation flip angle 15-degree, field of view (FOV) 4 or 3 cm, matrix dimension 128×128, slice thickness 1 mm, number of repetitions 2. To minimize the effect of the spatially dependent B1 produced by the surface coil, we tried to position the coil with the same distance from the injection site. A permanent marker was used to spot the needle track. In addition, after positioning of the coil we performed slice selective calibration of the 90-degree pulse. The slice with the hypointense signal from the grafted cells was selected based on gradient echo scout images.

SWIFT imaging

Phantom and *in vivo* SWIFT imaging were performed with the following parameters: RF excitation was performed with an amplitude- and frequency-modulated pulse of the hyperbolic secant (HS*n*) family [45] with stretching factor (*n*) of 2, a time-bandwidth product of 64. The pulse was oversampled by a factor of 16 [46]. Data were collected in 64 gaps in the HS*n* pulse, and after the pulse, 192 sample points were acquired without gaps. The bandwidths were 100 kHz and 62 kHz; readout times, 2.6 msec or 4 msec, excitation flip angle was varied from 1 to 22°; number of views 8192; number of averages 2; FOV 40 × 40 × 40 mm^3 *in vivo* and 60 × 60 × 60 mm^3 – in vitro, total scan time ~3 minutes. A magnetization preparation scheme with chemically selective pulses (duration 30 msec) was

applied in mice studies to suppress fat signal. After acquiring a full set of frequency-encoded projections, 3D images were reconstructed with CMRRpack v0.45b SWIFT software [47] using correlation and a 3D gridding algorithm with 0.156^3 mm^3 and 0.234^3 mm^3 isotropic voxel size for *in vivo* and *in vitro* experiments, respectively [48].

Quantification of imaging data

Quantifications of NMR signal were performed based on the estimation of longitudinal relaxation time (T1). T1 maps were reconstructed in Matlab using a variable flip angle method [37]. T1-color maps were created using ImageJ software (NIH image). A conversion of grey-scale into color images was performed with “spectrum” color map.

Results

1. Toxicity analysis of the iron oxide particles

Figure 1A shows the percentage of viable MSCs after overnight incubation of cells with different concentrations of iron oxide particles. The cell viability was not reduced (Figure 1A, black bars). At the same time, no substantial internalization of iron into the cells was detected by mass spectroscopy. A maximum of ~6 pg of iron per cell was found after MSCs incubation with 200 μg/ml of iron oxide in the media (Table1). The incubation of the MSCs with Feraheme-low-PLL mixture led to more than 3-fold increase in iron accumulation. A maximum ~22 pg of iron per cell was detected after overnight incubation with 200 μg/ml of iron oxide in the media (Table 1). No reduction in cell viability was detected in MSCs incubated with Feraheme-low-PLL mixture at iron concentrations up to 1000 μg/ml (Figure 1A gray bars). Incubation of MSCs with Feraheme-high-PLL mixture led to more than 20% reduction in cell viability at the iron concentration higher than 100 μg/ml of iron (Figure 1A, empty bars). Since Feraheme-low-PLL mixture did not produce toxic effects and led to higher iron accumulation in MSCs, we used this mixture in our future experiments.

To confirm that the Feraheme-low-PLL mixture did not cause any long-term toxicity of MSCs, we tested cell viability of iron oxide-labeled cells at 1, 5, 10 and 21 days after labeling. The cell viability remained the same as control/unlabeled cells with all Feraheme-low-PLL concentrations tested (Figure 1B). To further investigate the effect of Feraheme-low-PLL mixture on MSCs, we performed osteoblast differentiation of labeled MSCs. Optical analysis indicated that there was no difference in MSC differentiation into osteoblasts between the iron oxide-labeled MSCs and unlabeled MSCs. However, a small non-significant decrease in the number of differentiated cells was observed with increasing iron oxide concentrations (Figure 1C). Based on these data, we decided to use the labeling concentrations of iron oxide particles less than 400 μg/ml. From these *in vitro* experiments, we concluded that concentrations of Feraheme-low-PLL mixture in incubation media lower than 400 μg/ml had no adverse effect on MSCs viability, proliferation and osteoblast differentiation.

2. Generation of hyperintense signal from iron-labeled cells

2.1 Hyperintense signal from oxide solutions in a phantom—In the next experiments, we assessed the capacity of SWIFT sequence to generate a hyperintense signal

from iron-labeled cells. First, we performed imaging of the phantom with the iron oxide solutions. Figure 2 depicts SWIFT MR images of a phantom consisting of eight tubes with different concentrations (0 – 30 mg/ml) of iron oxide particles acquired at 2- (A), 10- (B) and 20-degree (C) excitation flip angles. The low flip angle acquisition provided a weak but detectable signal from pure water, while an increase of the flip angle led to a reduction of pure water signal and an increase in the signal intensity from the iron containing-solutions. Figure 2D depicts a graph of MRI signal intensity as a function of the excitation flip angle. Maximum signal intensity for a lower iron concentration (50 μg/m) was detected at a low flip angle (~10-degree), while a higher iron concentration (200 μg/m) required higher excitation flip angle (~15-degree) to reach a maximum. We utilized this property in our *in vivo* experiments to optimize the contrast between tissue and iron-labeled MSCs.

To determine the optimal concentration of the iron oxide particles for the generation of the hyperintense signal, we measured SWIFT MRI signal intensity from different concentrations of iron oxide at different excitation flip angles (Figure 2E). MRI signal increases initially, reaches a maximum and decreases again with increasing iron concentration. It is important to mention two issues related to this experiment: First, the version of SWIFT sequence and acquisition parameters we used in these experiments did not allow us to recover MRI signal from the vial with very high concentration of iron (30000 μg/ml). Second, a blurring of the images of the vials with high concentrations (≥300 μg/ml) of iron oxide particles was observed. To avoid blurry images from iron-labeled cells we decided to conduct our future labeling and imaging experiments with iron concentrations less than 300 μg/ml.

2.2 Hyperintense signal from iron oxide solution in muscle tissue—To confirm that hyperintense signal intensity can be reproduced *in vivo*, a solution of iron oxide particles was injected into muscle tissue of a mouse. Figure 3A shows gradient echo image of mouse hindlimb after the administration of 50 μl of 50 μg/ml of Feraheme solution. The signal void in the injection area was detected. Figure 3B shows SWIFT MR images of the same animal. The distinct hyperintense signal was observed at the injection site. The maximum contrast between muscle tissue and the iron solution was detected at ~10-degree excitation flip angle (Figure 3B).

2.3 Quantification of SWIFT signal from iron oxide solutions—Positive signal intensity allowed the quantification of iron oxide in the solution. We implemented variable flip angle method to produce an R1-map (R1~1/T1) of the phantom and correlated the concentration of iron oxide with the longitudinal relaxivity of Feraheme [37]. Figure 4A shows a SWIFT image of the phantom with low concentrations (less than 300 μg/ml at 2-degree excitation flip angle) of the iron oxide particles. No blurring of images was detected at these iron oxide concentrations. Figure 4B shows the R1-map of the phantom and Figure 4C shows T1-relaxivity vs. iron oxide concentrations. A linear relationship between iron oxide concentration and R1 was detected in this experiment (Figure 4C).

To ensure that the iron quantification could be performed *in vivo* we performed R1-mapping of mouse hindlimb after injecting 50 μl of 50 μg/ml iron oxide solution in the muscle (Figure 4D and 4E). The R1 value of the injected solution in the muscle tissue was compared with the R1 value of the calibration phantom (Figure 4C). R1 values from ROI of injected area

had a range of 3.8 – 0.6 (1/sec) with a mean value of 1.8 ± 0.8 (1/sec), while the R1 value of the same concentration of iron oxide solution in the phantom was 2.2 ± 0.1 (1/sec).

To make sure that the linear relationship between R1-relaxivity and the iron oxide concentration was maintained after internalization of the iron particles into the MSCs, we performed R1-mapping of the phantom with 1×10^6, 2×10^6 and 3×10^6 iron-labeled cells labeled with 18 pg per cell (labeling concentration of iron oxide 50 μg/ml). A linear dependence of R1-relaxivity on the concentration of iron-labeled cells was observed (Figure 4F).

2.4 Hyperintense signal from iron-labeled MSCs in vivo—To confirm that iron-labeled MSCs can be imaged with SWIFT pulse sequence *in vivo* and how long after injection these cells can be detected using MRI, we grafted 18×10^6 MSCs labeled with ~22 pg per cell (labeling solution of iron oxide 200 μg/ml) into muscle tissue of mouse hindlimb. SWIFT MR imaging was performed at ~1 hour, 3 days, 10 days and 19 days after injection. Figure 5A shows *in vivo* SWIFT MR image of a mouse hindlimb before the injection of iron-labeled MSCs. Imaging of the animal ~1 hour after the administration of labeled MSCs revealed very distinct hyperintense signal from the injection site at high excitation flip angles (Figure 5B). Maximum contrast (the difference between signal intensity from labeled cells and tissue) was detected at ~15-degree excitation flip angle. R1-mapping of tissue reviled the longitudinal relaxivity R1 = 2.7 ± 0.5 1/sec in the area of the injection. At day 3 after the implantation of the labeled MSCs (Figure 5C), the hyperintense signal had higher intensity with the maximum contrast at ~16-degree excitation flip angle and R1 = 3.3 ± 0.9 1/sec. At day 10 and 19, the intensity of the hyperintense signal from grafted cells gradually declined (Figure 5D and 5E). A maximum contrast was observed at flip angle of 10-degree (R1 = 2.3 ± 0.5 1/sec) and 6-degree (R1 = 1.9 ± 0.7 1/sec) for days 10 and 19, respectively. R1 values and corresponding iron concentrations from the injection sites at the different time points are shown in Figure 5F.

Discussion

Although T2*-weighted MRI has been used successfully for imaging of grafted cells [49], it produces a hypointense signal from iron-labeled cells, which makes their quantification and detection challenging in areas with low signal intensity, such as bone. In this study, we demonstrated that the SWIFT pulse sequence can produce a very distinct hyperintense signal from iron-labeled MSCs. We were able to follow and quantify the hyperintense signal from grafted cells for up to 19 days after administration of 18×10^6 MSCs labeled with ~ 22 pg per cell of iron into muscle tissue of mouse hindlimb. The proposed imaging and labeling protocols are useful for cell tracking studies since grafted cells can be readily observed and quantified.

Imaging of iron-labeled cells with SWIFT pulse sequence was reported earlier by Zhou et al. [38]. They demonstrated SWIFT imaging of a phantom with iron-labeled cells with distinct hyperintense signals; however, when the same cells were injected into mouse myocardium hypointense signal was observed with a marginal enhancement on magnitude images. The motivation for the current study was to improve this method and to generate a clear

hyperintense signal from grafted cell in the tissue. Below we offer a few tips for the selection of labeling and acquisition parameters to produce a hyperintense signal from iron-labeled donor cells and to quantify the imaging data.

Hyperintense signal from iron oxide particles

A distinct feature of the SWIFT sequence is that the excitation and acquisition of NMR signal have minimal separation: the acquisition delay (echo time) is about a few microseconds. Extremely short acquisition delay almost eliminates the T2 dependence of the MRI signal and makes SWIFT images primarily T1-weighted. With the SWIFT sequence, the intensity of the hyperintense signal from fast relaxing spins can be adjusted by varying the excitation flip angle. We demonstrated this capability in our phantom experiment with different iron oxide particle solutions (Figure 2). A suppression of pure water (long T1) signal and an increase in the signal intensity from the iron containing-solutions (short T1) upon the increase of the excitation flip angle were clearly observed in our study (Figure 2D). The maximum signal intensities for the solutions with different T1 were detected at different flip angles (Figure 2D). These flip angles are in an agreement with T1 relaxation times for the solutions and correlate with Ernst equation (data not shown). An optimization of the excitation flip angle in SWIFT sequence is a powerful approach to produce contrast between a tissue and grafted iron-labeled cells.

Optimal iron oxide concentration for the generation hyperintense signal with the SWIFT acquisition protocol

The success of the detection of iron-labeled cells in tissue with conventional $T2^*$-weighted MR imaging depends on the intracellular concentration of the contrast agent. The high intracellular concentration of the iron oxide accelerates the relaxation rate of nearby water protons and a larger area of signal void appears on MR images. In our previous experiments, we attempted to maximize intracellular iron uptake and were limited only by the ability of cells to uptake iron oxide and the toxic effect of the contrast media [42]. Generation of the hyperintense signal from iron-labeled cells with the SWIFT acquisition protocol applies an additional limitation. When the concentration of iron oxide becomes too high the signal intensity starts to decline (Figure 2E). The reduction of the signal intensity at high iron concentration is due to the extreme acceleration of the T2 relaxation rate. When T2 becomes comparable or shorter than the acquisition dwell time (~ 1/bandwidth) the signal intensity begins to decrease [50] (Figure 2E). In addition to the reduction of the signal intensity, extreme short T2 also leads to the broadening of the point spread function [28] and blurring of the image. In our phantom experiments, we observed image blurring at iron concentrations higher than 300 μg/ml while the vial with 30,000 μg/ml solution was not visible at all (Figure 2A–C). Acquisition with higher bandwidth reduces blurring and allowed the detection of a signal with shorter T2 [51]. To ensure that our *in vivo* images would not have blurring artifacts we decided to use the labeling concentration of iron oxide lower than 300 μg/ml and acquired images with 100kHz bandwidth.

Effect of iron oxide particles on MSCs

Another factor which we considered when choosing the labeling concentration of iron oxide was the toxic effect of the particles on MSCs. Pre-incubation of MSCs with Ferahem-low-

PLL mixture resulted in the internalization of up to ~22 pg of Fe per cells with no reduction in proliferation, differentiation or viability of MSCs. A similar level of labeling of MSCs was reported earlier after pre-incubation of iron oxide with PLL [40] or protamine sulfate [52]. A ten-fold increase in the concentration of the transfection agent led to substantial reduction of cell viability. Twenty percent of the cell death was observed after overnight incubation of MSCs with 100 μg/ml of iron oxide and 7.5 μg/ml of PLL mixture. To minimize the toxic effect of the contrast agent and transfection agent on donor cells we used the labeling protocol with the low concentration of PLL.

Quantification of SWIFT imaging data

We utilized linear dependence of the iron oxide concentration and R1-relaxivity to quantify the amount of iron in the tissue after administration of the iron oxide solution in muscle tissue (Figure 4C). Reasonable agreement with the calibration curve was detected (Figure 4C and E). A wide distribution of R1 values in the tissue was detected: 3.8 – 0.6 1/sec. Close examination of the injected area revealed that the central part of the injection area has pixels with higher relaxivity than pixels on the periphery.

There are two main factors affecting the longitudinal relaxation in the presence of paramagnetic centers which are: 1) the surface area of the particle - liquid interface and 2) the diffusion capability of protons [53]. Water protons in the heterogeneous tissue must overcome several obstacles (cells membranes, floating macromolecules, different viscosity and others) to interact with iron oxide particles, while in the homogenous aqueous solution iron oxide particles are readily accessible for the interaction with protons. This difference in accessibility of protons (lower diffusion) may change the relaxivity of iron oxide in the tissue. Aggregation of the iron oxide particles might be another reason for R1 heterogeneity in the tissue (smaller surface area). Additional information about quantification of iron oxide in the tissue can be found in other publication from our group [54].

We also investigated the R1-relaxivity of the iron oxide after internalization of this particle into MSCs. In the phantom with different amounts of iron-labeled cells, a linear dependence was detected (Figure 4F). The linear dependence of R1-relaxivity on the number of the labeled cells indicates that the variable flip angle method can be utilized for the quantitation of labeled cells' dilution. However, further experiments are needed to determine the R1-relaxivity of iron-labeled cells in the tissue and determine that this relaxivity is time independent.

Longitudinal detection of iron-labeled cells

The goal of our final experiment was to confirm that the proposed protocols allow the detection of iron-labeled MSCs. We were also interested to determine how long after injection, the iron-labeled cells can be identified and to quantify with SWIFT imaging. A distinct hyperintense signal from iron-labeled MSCs was observed for 19 days after implantation of 18×10^6 cells (Figure 5A–E). Similar results were reported previously [42], but with the hypointense signal from grafted cells. For the quantification of the iron oxide in the muscle tissue after administration of labeled MSCs, we utilized the calibration obtained in the iron solution experiment (Figure 4C). The lower R1 (R1=2.7 ± 0.5 1/sec) value 1 hour

after injection is probably due to partial volume averaging effect: long T1 signal from PBS (used to re-suspend the labeled cells), partially masked the short T1 signal from iron-labeled cells. After 3 days, the PBS most likely diffused out from the injection area and the remaining cells revealed higher hyperintense signal (R1 = 3.3 ± 0.9 1/sec). The recalculation of T1-relaxivity into the iron concentration revealed the presence of approximately of 62 μg/ml of Fe in the injected area at 1 hour after injection and 80 μg/ml of Fe at day 3. The gradual decrease of R1 values in the injected area was observed from day 3 to day 19 after injection, which corresponds to the further reduction of the iron concentration from 52 μg/ml to 43 μg/ml of Fe. The decrease of iron concentration in the injected area can be attributed to the death of grafted cells and uptake/removal of the iron oxide particles by immune cells. A dilution of the intracellular iron due to migration of the labeled cells from the injection site also can contribute to this decrease. The delineation of all possible reasons for the degradation of MRI signal from injected cells overtime required more systematic biological experiments and is beyond the scope of this study.

The recent publication by Wang et al. [55] provided a scheme to suppress signals from fat and tissues with long T2. Two additional RF pulses were suggested to accomplish this goal and images with an improved contrast between the host tissue and the injected iron oxide particles were presented. In our work, we suggested a different strategy. Acquisition of images with higher flip angles (flip > 10°) provided a better contrast/visibility of grafted solution, while low flip angle images (flip < 10°) provided better anatomical representation of the tissue (Figure 3). This strategy can reduce the total acquisition time, simplifies sequence and eliminates potential problems associated with ghosting due to additional RF excitation.

Also, one of the limitations of conventional T2*-weighted imaging for the detection of iron labeled cells is inability to distinguish donor cells and hemosiderin. We did not have a chance to investigate in detail appearance of a hemosiderin on SWIFT images. However, our preliminary experiments have shown that hemorrhages appears dark on SWIFT images at flip angels range from 5 to 25-degree. This would be an advantage of the proposed method, since it will allow to differentiate grafted cells (hyperintense signal) and hemosiderin (hypointense signal). However, more systematic studies are needed to determine optimal imaging parameters.

There are several weaknesses in our experimental design. For the quantification of the amount of iron in the tissue, we made several assumptions: 1) that the R1-relaxivity of the iron-labeled cells in the tissue is not significantly different compared to the aqueous solution (Figure 4 C). 2) Relaxivity or iron labeled cells remained constant at different days post-injection. These assumptions have to be tested and corrections may be applied.

The goal of our labeling protocol was to create a unique R1-signature of the donor cells, which will clearly differentiate them from host tissue on R1-map. Our experiment with the bolus injection of iron labeled MSCs showed that it is possible for the muscle tissue. However, more optimization will be needed to image grafted cells injected into different organs. Also, we utilized the simplest model of cells implantation, which did not describe complicated processes of extensive migration and differentiation of grafted cells into

different types of tissues. Therefore, the time period when the labeled cells can be detected could vary significantly in more advance animal model of cell therapy.

The main goal of this study was to demonstrate the feasibility of hypointense signal intensity generation and quantification of the iron-labeled MSCs overtime. To minimize problems associated with the detection of a small amount of cells, we performed our experiments with the large number of cells (18×10^6). Usually, in preclinical studies, lower number of cells (1–10 million) is administered to an animal. We were able to detect very clear hyperintense signal from 5×10^6 cells in the muscle tissue of mice one hour after injection (data not shown) but did not follow this graft overtime. Additional experiments are needed to determine the efficacy of MSC detection and quantification when fewer cells are injected in an animal model with wider migration capabilities of grafted cells.

In order to increase SNR and reduce background signal from the coil itself, we performed our *in vivo* experiments with a 2 cm surface coil. Inhomogeneity of B1 field produced by a surface coil can cause errors in the determination of R1 [37]. To minimize the influence of variation in B1 field, we tried to position the coil in such a way that the injection area had the same distance to the coil and presumably experienced the same flip angle. We also performed slice selective calibration of the 90-degree pulse. This setup is not optimal, and it is more desirable to use volume coils with a homogeneous B1 field, which we will utilize in our future experiments. It is also important to mention that most commercial coils have plastic elements which become NMR visible with SWIFT acquisition. This background signal can cause substantial image distortions.

Conclusion

In our study, we have shown that the SWIFT pulse sequence allowed the generation of a quantifiable MRI signal from iron-labeled MSCs. Overnight incubation of MSCs with a Feraheme-low-PLL mixture at the concentration less than 300 μg/ml of iron oxide did not alter long- and short-term proliferations, osteoblast differentiation of the cells or blurring of MR images. Incubation of MSCs with 200 μg/ml of iron oxide lead to the accumulation of 22 pg of iron oxide per cell. This intracellular concentration was sufficient to generate a distinct quantifiable hyperintense signal from the graft with the SWIFT pulse sequence. This MRI signal was detected up to 19 days after the injection of 18×10^6 cells into the muscle tissue of mouse hindlimb. The excitation flip angle of SWIFT sequence can be used for the optimization of the contrast between tissue and iron-labeled cells. This angle depends on T1s of iron-labeled cells and tissue. Results obtained in this study are the first steps in developing a noninvasive imaging method to monitor a stem cell therapy of bone disorders.

Acknowledgments

Research reported in this publication was supported by the National Institute of Arthritis and Musculoskeletal and Skin Diseases of the National Institutes of Health under Award P50 AR060752, R01 AR043052 and 5K24AR048841-11 (NEL), R21 AR068507 (SM) and P41 EB015894. The content is solely the responsibility of the authors and does not necessarily represent the official views of the National Institutes of Health. We also would like to thank Sergio B Wong and Tony Huynh for the help with MRI acquisition and animal preparations.

References

1. Pittenger MF, et al. Multilineage potential of adult human mesenchymal stem cells. Science. 1999; 284(5411):143–147. [PubMed: 10102814]
2. Watson L, Elliman SJ, Coleman CM. From isolation to implantation: a concise review of mesenchymal stem cell therapy in bone fracture repair. Stem Cell Res Ther. 2014; 5(2):51. [PubMed: 25099622]
3. Bornes TD, Adesida AB, Jomha NM. Mesenchymal stem cells in the treatment of traumatic articular cartilage defects: a comprehensive review. Arthritis Res Ther. 2014; 16(5):432. [PubMed: 25606595]
4. Yao W, Lane NE. Targeted delivery of mesenchymal stem cells to the bone. Bone. 2015; 70:62–65. [PubMed: 25173607]
5. Guan M, et al. Directing mesenchymal stem cells to bone to augment bone formation and increase bone mass. Nat Med. 2012; 18(3):456–462. [PubMed: 22306732]
6. Naumova AV, et al. Clinical imaging in regenerative medicine. Nat Biotechnol. 2014; 32(8):804–818. [PubMed: 25093889]
7. Shapiro EM, et al. In vivo detection of single cells by MRI. Magnetic Resonance in Medicine. 2006; 55(2):242–249. [PubMed: 16416426]
8. de Vries IJ, et al. Magnetic resonance tracking of dendritic cells in melanoma patients for monitoring of cellular therapy. Nat Biotechnol. 2005; 23(11):1407–1413. [PubMed: 16258544]
9. Zhu J, Zhou L, XingWu F. Tracking neural stem cells in patients with brain trauma. N Engl J Med. 2006; 355(22):2376–2378. [PubMed: 17135597]
10. Callera F, de Melo CM. Magnetic resonance tracking of magnetically labeled autologous bone marrow CD34+ cells transplanted into the spinal cord via lumbar puncture technique in patients with chronic spinal cord injury: CD34+ cells' migration into the injured site. Stem Cells Dev. 2007; 16(3):461–466. [PubMed: 17610376]
11. Toso C, et al. Clinical magnetic resonance imaging of pancreatic islet grafts after iron nanoparticle labeling. Am J Transplant. 2008; 8(3):701–706. [PubMed: 18294167]
12. Stuber M, et al. Positive contrast visualization of iron oxide-labeled stem cells using inversion-recovery with ON-resonant water suppression (IRON). Magn Reson Med. 2007; 58(5):1072–1077. [PubMed: 17969120]
13. Vonken EJ, et al. Direct in vitro comparison of six three-dimensional positive contrast methods for susceptibility marker imaging. J Magn Reson Imaging. 2013; 38(2):344–357. [PubMed: 23281151]
14. Eibofner F, et al. Utilizing echo-shifts in k-space for generation of positive contrast in areas with marked susceptibility alterations. Magn Reson Med. 2012; 68(5):1399–1409. [PubMed: 22183853]
15. Mani V, et al. Gradient echo acquisition for superparamagnetic particles with positive contrast (GRASP): sequence characterization in membrane and glass superparamagnetic iron oxide phantoms at 1.5T and 3T. Magnetic Resonance in Medicine. 2006; 55(1):126–135. [PubMed: 16342148]
16. Bergin CJ, Glover GH, Pauly JM. Lung parenchyma: magnetic susceptibility in MR imaging. Radiology. 1991; 180(3):845–848. [PubMed: 1871305]
17. Gatehouse PD, Bydder GM. Magnetic resonance imaging of short T2 components in tissue. Clin Radiol. 2003; 58(1):1–19. [PubMed: 12565203]
18. Boujraf S, et al. Ultrafast bold fMRI using single-shot spin-echo echo planar imaging. J Med Phys. 2009; 34(1):37–42. [PubMed: 20126564]
19. Bracher AK, et al. Feasibility of ultra-short echo time (UTE) magnetic resonance imaging for identification of carious lesions. Magn Reson Med. 2011; 66(2):538–545. [PubMed: 21360742]
20. Hafner S. Fast imaging in liquids and solids with the Back-projection Low Angle ShoT (BLAST) technique. Magn Reson Imaging. 1994; 12(7):1047–1051. [PubMed: 7997092]
21. Madio DP, Lowe IJ. Ultra-fast imaging using low flip angles and FIDs. Magn Reson Med. 1995; 34(4):525–529. [PubMed: 8524019]

22. Weiger M, Pruessmann KP, Hennel F. MRI with zero echo time: hard versus sweep pulse excitation. Magn Reson Med. 2011; 66(2):379–389. [PubMed: 21381099]
23. Weiger M, et al. High-resolution ZTE imaging of human teeth. NMR Biomed. 2012; 25(10):1144–1151. [PubMed: 22290744]
24. Grodzki DM, Jakob PM, Heismann B. Ultrashort echo time imaging using pointwise encoding time reduction with radial acquisition (PETRA). Magn Reson Med. 2012; 67(2):510–518. [PubMed: 21721039]
25. Idiyatullin D, et al. Fast and quiet MRI using a swept radiofrequency. J Magn Reson. 2006; 181(2): 342–349. [PubMed: 16782371]
26. Carl, M., et al. ISMRM Annual Scientific Meeting & Exhibition. Stockholm, Sweden: 2010. Bloch Simulations of UTE, WASPI and SWIFT for Imaging Short T2 Tissues.
27. Weiger M, et al. High-resolution ZTE imaging of human teeth. NMR in Biomedicine. 2012; 25(10):1144–1151. [PubMed: 22290744]
28. Rahmer J, et al. Three-dimensional radial ultrashort echo-time imaging with T2 adapted sampling. Magn Reson Med. 2006; 55(5):1075–1082. [PubMed: 16538604]
29. Idiyatullin D, et al. Dental magnetic resonance imaging: making the invisible visible. J Endod. 2011; 37(6):745–752. [PubMed: 21787482]
30. Kendi AT, et al. Transformation in mandibular imaging with sweep imaging with fourier transform magnetic resonance imaging. Arch Otolaryngol Head Neck Surg. 2011; 137(9):916–919. [PubMed: 21930980]
31. Idiyatullin D, et al. Continuous SWIFT. J Magn Reson. 2012; 220:26–31. [PubMed: 22683578]
32. Idiyatullin D, et al. Gapped pulses for frequency-swept MRI. J Magn Reson. 2008; 193(2):267–273. [PubMed: 18554969]
33. Idiyatullin D, et al. Role of MRI for detecting micro cracks in teeth. Dentomaxillofac Radiol. 2016; 45(7):20160150. [PubMed: 27402200]
34. Kobayashi N, et al. SWIFT MRI enhances detection of breast cancer metastasis to the lung. Magn Reson Med. 2015; 73(5):1812–1819. [PubMed: 24919566]
35. Lehto LJ, et al. Detection of calcifications in vivo and ex vivo after brain injury in rat using SWIFT. Neuroimage. 2012; 61(4):761–772. [PubMed: 22425671]
36. Wang L, et al. T(1) estimation for aqueous iron oxide nanoparticle suspensions using a variable flip angle SWIFT sequence. Magn Reson Med. 2013; 70(2):341–347. [PubMed: 23813886]
37. Zhang J, et al. Quantifying iron-oxide nanoparticles at high concentration based on longitudinal relaxation using a three-dimensional SWIFT Look-Locker sequence. Magn Reson Med. 2014; 71(6):1982–1988. [PubMed: 24664527]
38. Zhou R, et al. SWIFT detection of SPIO-labeled stem cells grafted in the myocardium. Magn Reson Med. 2010; 63(5):1154–1161. [PubMed: 20432286]
39. Frank JA, et al. Magnetic intracellular labeling of mammalian cells by combining (FDA-approved) superparamagnetic iron oxide MR contrast agents and commonly used transfection agents. Academic Radiology. 2002; 9(Suppl 2):S484–S487. [PubMed: 12188316]
40. Frank JA, et al. Clinically applicable labeling of mammalian and stem cells by combining superparamagnetic iron oxides and transfection agents. Radiology. 2003; 228(2):480–487. [PubMed: 12819345]
41. Bulte JW, et al. Preparation of magnetically labeled cells for cell tracking by magnetic resonance imaging. Methods Enzymol. 2004; 386:275–299. [PubMed: 15120257]
42. Magnitsky S, et al. In vivo and ex vivo MRI detection of localized and disseminated neural stem cell grafts in the mouse brain. Neuroimage. 2005; 26(3):744–754. [PubMed: 15955483]
43. Shapiro EM, et al. MRI detection of single particles for cellular imaging. Proc Natl Acad Sci U S A. 2004; 101(30):10901–10906. [PubMed: 15256592]
44. Gregory CA, et al. An Alizarin red-based assay of mineralization by adherent cells in culture: comparison with cetylpyridinium chloride extraction. Anal Biochem. 2004; 329(1):77–84. [PubMed: 15136169]
45. Tannus A, Garwood M. Improved Performance of Frequency-Swept Pulses Using Offset-Independent Adiabaticity. Journal of Magnetic Resonance. 1996; A 120(1):133–137.

46. Idiyatullin D, et al. Gapped pulses for frequency-swept MRI. Journal of Magnetic Resonance. 2008; 193(2):267–273. [PubMed: 18554969]
47. SWIFT software. Available from: http://www.cmrr.umn.edu/swift
48. Beatty PJ, Nishimura DG, Pauly JM. Rapid gridding reconstruction with a minimal oversampling ratio. Medical Imaging, IEEE Transactions on. 2005; 24(6):799–808.
49. Magnitsky S, et al. Magnetic resonance imaging as a tool for monitoring stem cell migration. Neurodegenerative Diseases. 2007; 4(4):314–321. [PubMed: 17627135]
50. Idiyatullin D, et al. Fast and quiet MRI using a swept radiofrequency. Journal of Magnetic Resonance. 2006; 181(2):342–349. [PubMed: 16782371]
51. Idiyatullin D, et al. Continuous SWIFT. Journal of Magnetic Resonance. 2012; 220(0):26–31. [PubMed: 22683578]
52. Arbab AS, et al. Labeling of cells with ferumoxides-protamine sulfate complexes does not inhibit function or differentiation capacity of hematopoietic or mesenchymal stem cells. NMR in Biomedicine. 2005; 18(8):553–559. [PubMed: 16229060]
53. Foley II, Farooqui SA, Kleinberg RL. Effect of Paramagnetic Ions on NMR Relaxation of Fluids at Solid Surfaces. J Magn Reson A. 1996; 123(1):95–104. [PubMed: 8980068]
54. Zhang J, et al. Quantification and biodistribution of iron oxide nanoparticles in the primary clearance organs of mice using T1 contrast for heating. Magn Reson Med. 2016
55. Wang L, et al. Improving detection specificity of iron oxide nanoparticles (IONPs) using the SWIFT sequence with long T(2) suppression. Magn Reson Imaging. 2014; 32(6):671–678. [PubMed: 24666573]

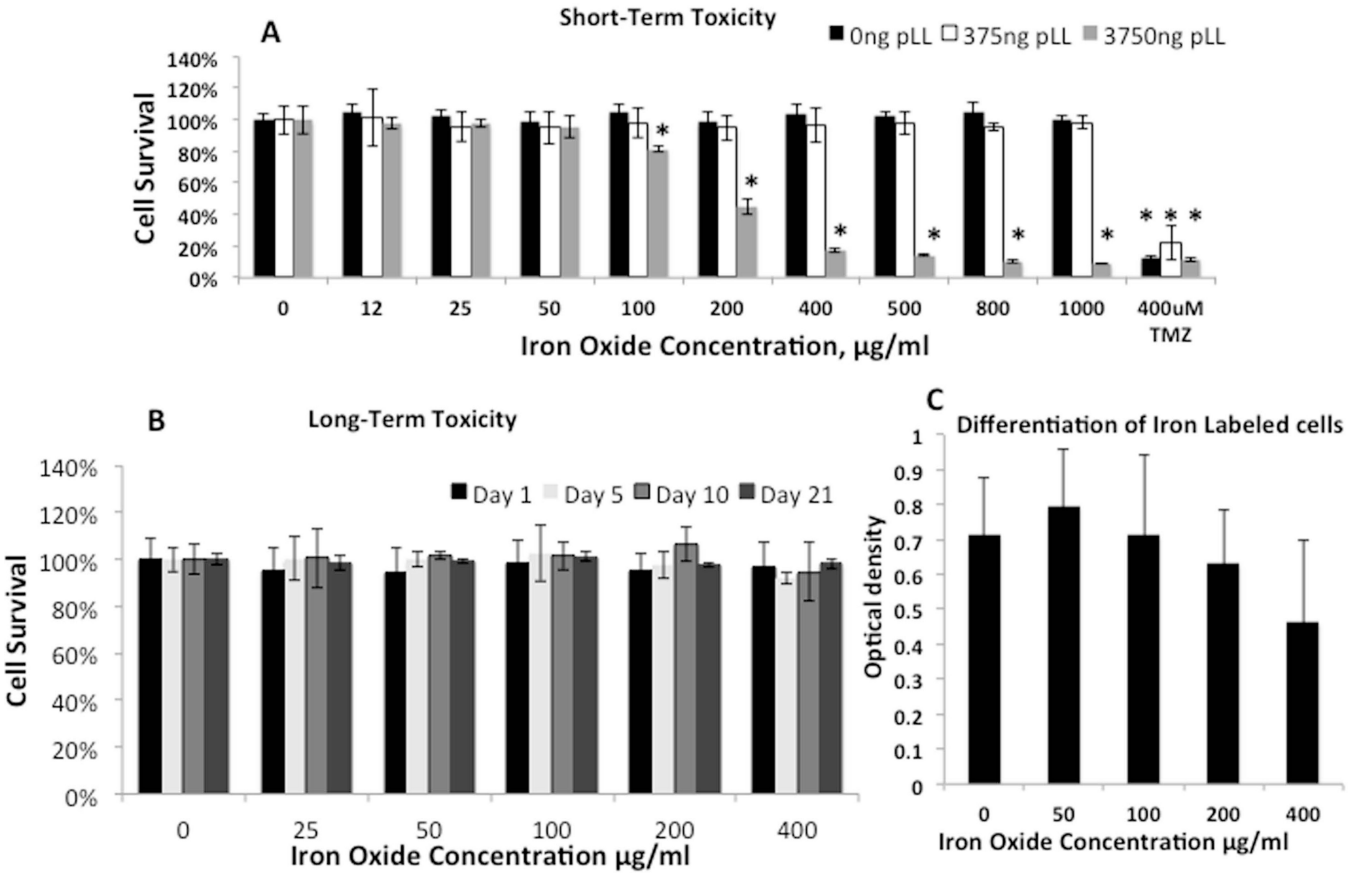

Figure 1. Toxicity test of iron oxide particles (FeOx) and Poly-L-Lysine (PLL) on Mesenchymal Stem Cells (MSCs)

(A) - Percentage of viable MSCs after overnight incubation with different concentrations of FeOx (black bars) and (FeOx/PLL) mixtures: White bars – FeOx-Low-PLL (each 50 µg/ml of FeOx were mixed with 375 ng of PLL), Gray bars – FeOx-High-PLL (each 50 µg/ml of FeOx were mixed with 3750 ng of PLL)

(B) - Percentage of viable MSCs, labeled with different concentration of FeOx-Low-PLL, after 1, 5, 10, and 21 days of proliferation.

(C) – Quantification of Alizarin Red staining of FeOx-Low-PLL labeled MSCs after 21 days of incubation in a differentiation media.

Concentrations of FeOx-Low-PLL less than 400 µg/ml are safe and can be used for the labeling of MSCs.

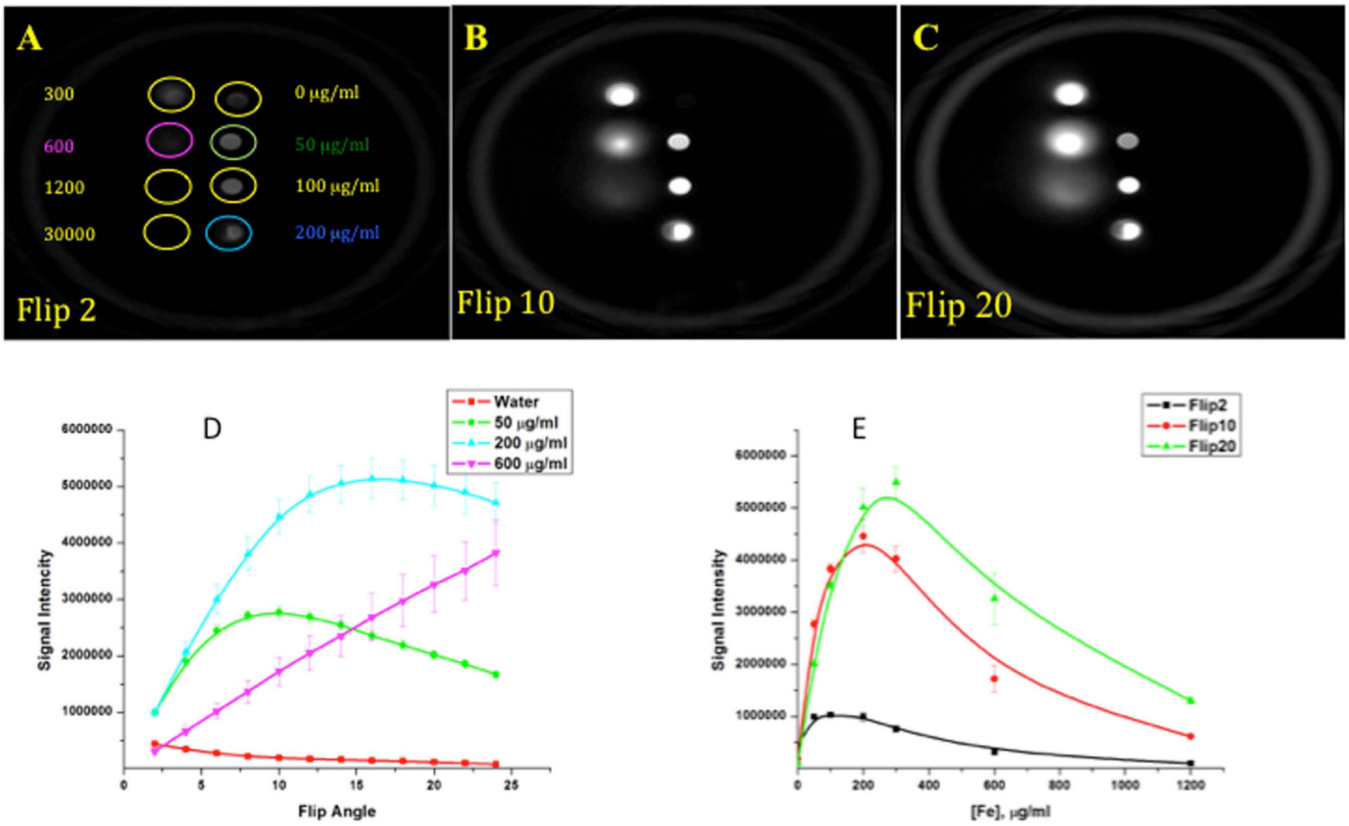

Figure 2. SWIFT MR images of the phantom with different concentrations of iron oxide particles solutions

(A, B, C) – SWIFT images (acquisition bandwidth 64kHz) of the phantom acquired at 2, 10 and 20-degree excitation flip angles.

(D) - SWIFT signal intensity as a function of the excitation flip angle of different concentrations of iron oxide particles. Each iron concentration curve reaches a maximum at definite excitation flip angles.

(*E*) – SWIFT signal intensity vs. iron oxide concentrations at different excitation flip angles. SWIFT pulse sequence generates hypointense MRI signal from iron oxide particles.

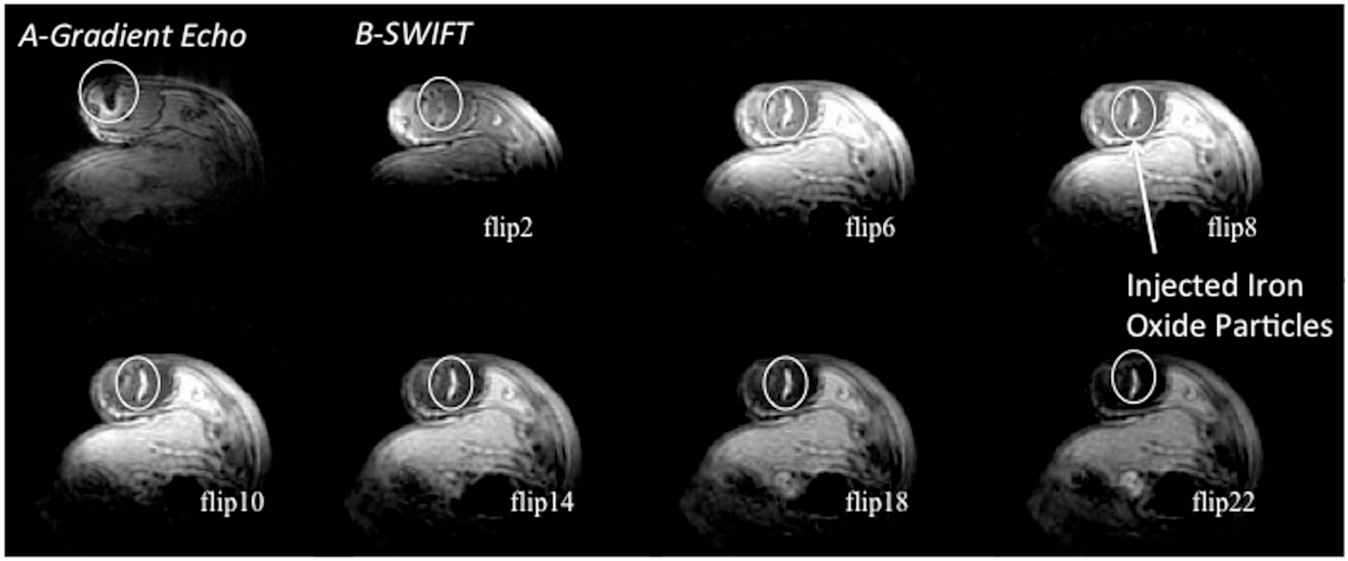

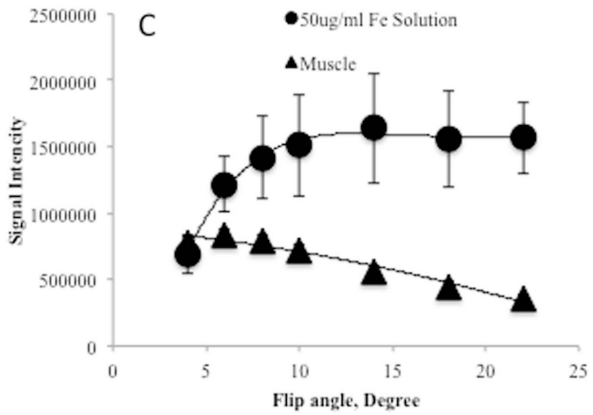

Figure 3. MR images of mouse hindlimb after administration iron oxide solution

(A) – Gradient echo image of mouse hindlimb after administration of 50 μl of 50 μg/ml of the iron oxide solution. Circle is a hypointense area from iron labeled cells.

(B)- SWIFT images of the same hindlimb (A) acquired at different excitation flip angles. Hyperintense signal reached the maximum at ~ 10-degree excitation flip angle.

(C)– Signal intensity of the tissue and the injected site at different excitation flip angle. SWIFT pulse sequence generates hyperintense MRI signal from iron oxide solution in tissue.

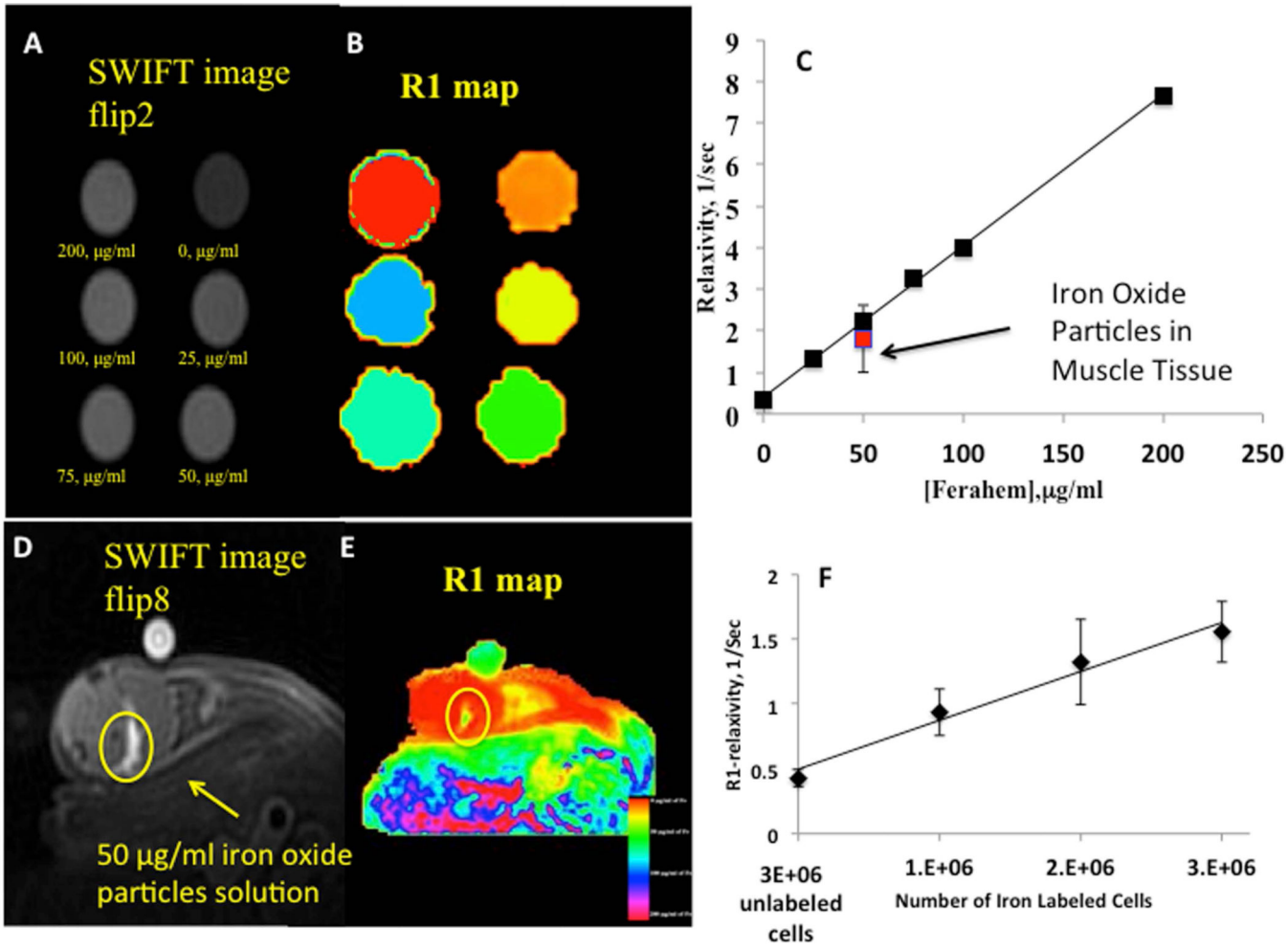

Figure 4. Quantification of SWIFT MRI signal

(A)– SWIFT MR image (flip angle-2°, acquisition bandwidth 100kHz) of the phantom with different concentrations of iron oxide solution acquired with 2-degree excitation flip angle.

(B)– R1 map of the phantom generated with variable flip angle method

(C)– Longitudinal relaxivity as a function of the iron oxide concentration. Error bars smaller than symbols. The linear dependence of R1 vs. the iron oxide concentration can be used for the quantification of the iron amount in a tissue.

(D)- SWIFT MR image (flip angle-8°, acquisition bandwidth 100kHz) of the mouse hindlimb acquired one hour after injection of 50 μl of 50 μg/ml of the iron oxide solution.

(E)- R1 map of the mouse hindlimb from the panel (D).

(F)- R1-relaxivity as a function of the number of iron labeled MSCs. The linear dependence of R1-relaxivity on the number of the labeled cells indicates that the variable flip angle method can be utilized for the quantitation of labeled cells' dilution.

Variable flip angle method provides correct estimation of the iron oxide in the tissue

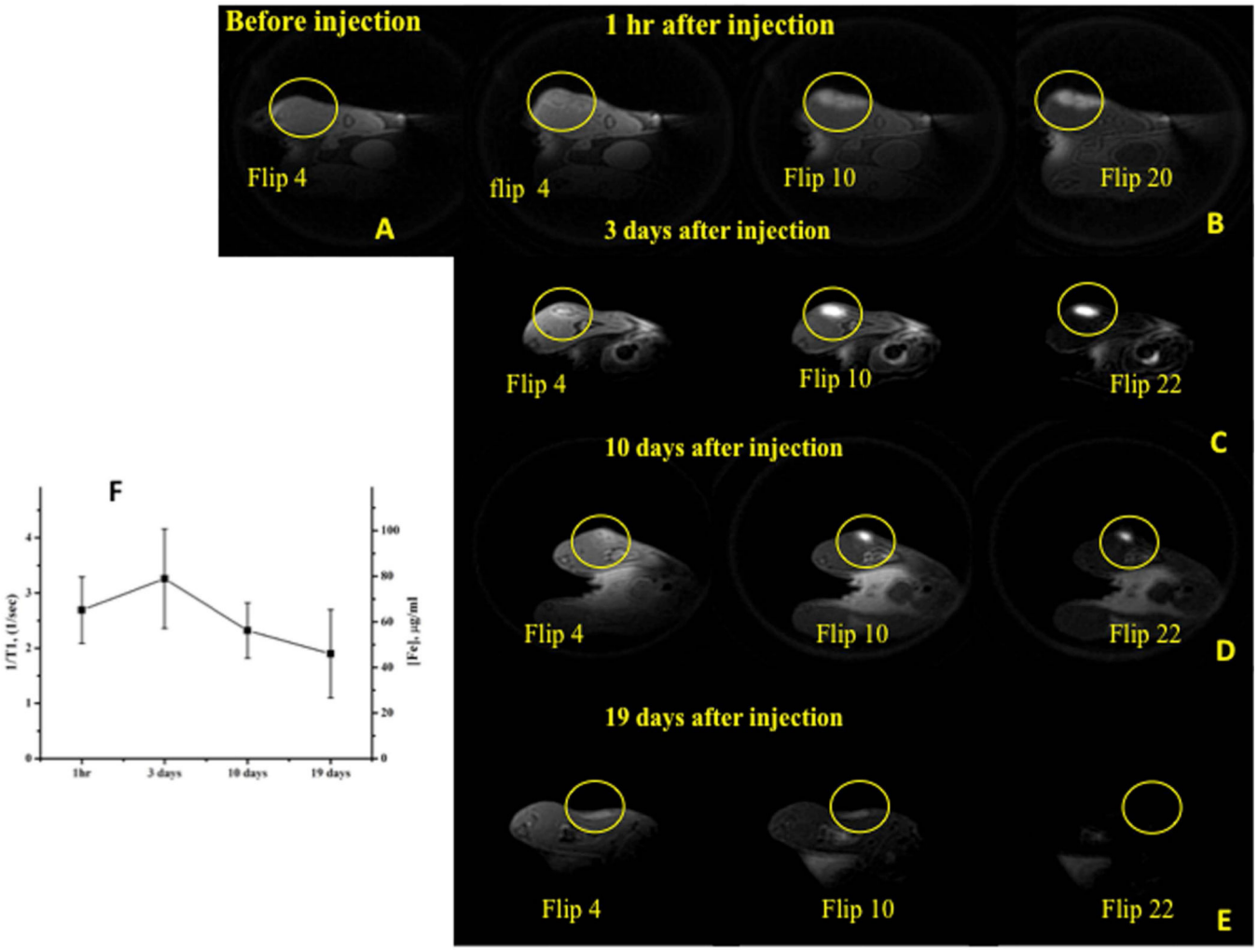

Figure 5. Longitudinal SWIFT MRI detection and quantification of iron labeled MSCs in muscle tissue

(A)- SWIFT MR image of mouse hind limb before injection of iron labeled MSCs

(B)– SWIFT MR images of mouse hind limb 1 hour after administration of 18×10^6 MSCs labeled with ~22 pg of iron per cell and re-suspended in 100 μl of PBS.

(C, D, F) - SWIFT MR images of mouse hindlimb at 3,10 and 19 days after administration of labeled MSCs. The distinct hyperintense signal from grafted cells was detected for 19 days.

(G)– R1 values of the injection site at 1 hour and 3,10, 19 days after administration of the iron labeled MSCs. Color images of the right are corresponding R1 maps.

SWIFT imaging allowed detection of the hyperintense signal from grafted iron labeled cells and quantitate the amount of iron in the site of injection.

Table 1

Intracellular iron concentration after overnight incubation of MSCs with different concentrations of Feraheme-PLL.

	Iron Oxide particles Concentration in Media (μg/ml)			
Poly-L-Lysine (ng/ml)	**25**	**50**	**100**	**200**
0	1.48 ± 0.15	2.26 ± 0.06	3.11 ± 0.05	6.21 ± 1.89
375	17.9 ± 1.77	18.0 ± 0.59	17.0 ± 1.09	22.3 ± 1.18